Defining a Harmonic Potential Well in a Linear Paul Trap

Ryan McGill
Research Scientist
Quantum Systems Division
Georgia Tech Research Institute

***Abstract*—Linear Paul traps provide a simple geometry for trapping Calcium ions. The equation for motion and velocity of the ion in these traps take the form of Mathieu's equation, which has exact analytical and known numerical solutions. All trap geometries are built around parameters from this equation, which include the necessary applied voltages, electrode distance, and more. However, not all solutions to the Mathieu equation remain stable at long integration times, which would lead to particle motion exponentially increasing in time and thus ejecting the ion from the potential well. Therefore, numerical analysis of the Mathieu equation is necessary to determine stable solutions to the Mathieu equation and to advise the design of a trap. First, an Ince-Strutt stability diagram is found in order to determine stable parameters for the Mathieu equation in Hill form. Next, an analysis of bounded and unbounded particle motion is examined for certain parameter values from the Ince-Strutt results to further prove stability. With this proof, a linear Paul trap geometry is defined, and electrostatic potentials are simulated using Poisson's equations. The results of each simulation are discussed, including the numerical solving methods used at each step. Limitations and improvements are included on how to both strengthen assertions about accuracy as well as improve design.**

I. Background

Ion traps serve as an "experimental playground" for physics experiments. The atomic source used for traps have the ability to serve as a sensor (spectroscopy, magnetometry [1]) or as a qubit for a quantum computer [2]. In short, trapping involves taking an atomic source, ejecting an electron for ionization, and then creating an electric potential field to confine the single ion. The equations which discussed in this work have been around for some time, but it wasn't until the 1990s that the modernization of hardware caught up to the math to finally allow the efficient use of ion traps in both academia and industry [3].

Nonetheless, the majority of today's ion traps are compact, microfabricated chips that provide the electric and magnetic confining potentials [4]. Macro-traps, sometimes termed dust traps, focus on large particles that are charged via friction and static voltages, and can often times be viewed with the naked eye. Micro-traps are built to handle charged particles at the atomic level, operating on single ions to chains or "crystals" of ions [5], typically under high vacuum. For quantum computing, it is often the case that the trap is also cooled down to very low temperatures (down to 5 Kelvin) in order to reduce thermal noise which produce lossy measurements [6]. Micro-traps are the focus of this work, though the fundamental concepts can be extended to most macro-traps. An example of a microfabricated trap used in GTRI's lab is shown in Figure 1.

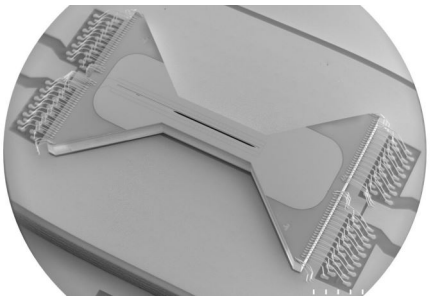

Fig. 1. A scanning electron microscope image of a microfabricated surface electrode Phoenix trap [7]. Image source: arXiv.

A. Operating an Ion Trap

In order to understand the importance of the trapping potential, it is helpful to walk through the process of loading an ion. While many atomic species are viable for trapping, this paper focuses on $^{40}Ca^{+}$ (hereon designated by Ca^{+}) ions as they are a popular atomic source for their long lived qubit state, as well as used in many of the labs located on Georgia Tech's campus.

The first step is to turn the Calcium source from a solid to a gaseous state. Calcium rocks are loaded into a copper tube that is placed near the trap surface, crimped on the edges to prevent spillage and cut with a slit for ejecting the atoms. A DC power supply applies power across the tube, heating up the source and sublimating Calcium through the slit and above the trap surface [8].

Next, two lasers containing 423nm and 375nm wavelength light illuminate a desired spot above the trap surface. These beams photoionize Calcium and give the desired charged particle, Ca^{+}.

Finally, an electric potential well is used to confine the newly charged particle above the trap surface. This is done in a variety of ways, and are the focus of this project.

B. Types of Trapping Potentials

There are two definitive methods of creating electrical potential wells for ion traps. They differ in both construction

and electrical modulation, and are defined in the following subsections.

1) Penning Traps: Penning traps use a strong magnetic field and static electric field to create the trapping potential for the ion [9]. This type of trap is not be derived in this project, but is mentioned for posterity.

2) Paul Traps: Earnshaw's theorem states that a charged particle can never act as a sole confining potential [10]. Ergo, DC electric fields are not enough to keep an ion in a single, "trapped" potential well above the trap surface. The solution developed by Wolfgang Paul is to apply an alternating pulse (typically an RF signal) that creates an average confining potential for the particle [11]. It can be envisioned as an atomic tug-of-war; when the RF is at its peak, the particle is repelled. At the minimum, the RF source electrode will attract the Ca^{+}, bringing it back to its original place.

These electrical geometries can be realized using rods in 3D space (known as a linear trap), in cylinders (called cylindrical traps), or, and most commonly, as a planar trap. Planar traps are microfabricated and use RF and DC electrodes located on the surface. For the derivations in this paper, the focus is on a linear trap, as the equations for most other traps attempt to approximate the same potential scheme.

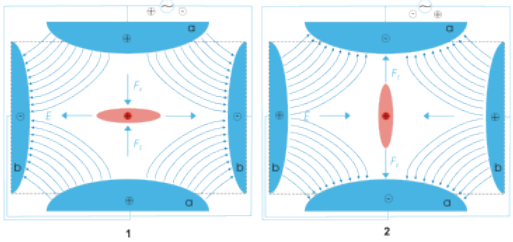

Fig. 2. Field diagram of an electric quadrupole. The left and right images show the RF electrodes when the amplitudes are 180 deg out of phase or after half a period has passed. Image source: Wikipedia.

II. Introduction

A. Trapping Potentials and the Mathieu Equation

Consider a setup with four, equally spaced rods that can be charged with DC and RF voltages. Figure 2 is a depiction of such a setup. The potential at the center of the trap can be modeled in a variety of ways, but for simplicity the following form is used [12]:

$$\Phi(t,x,y) = (\Phi_{dc} + \Phi_{ac}\cos(\Omega_{RF}t))\frac{x^2-y^2}{2r_0} \tag{1}$$

where r_0 is the distance from the rods to the center of the trap, x and y are Cartesian coordinates of the potential, Φ_{dc} and Φ_{ac} are the DC voltage and RF voltage amplitudes (respectively), and Ω_{RF} is the angular frequency of the RF field.

Consider a particle with charge e and mass m. The particle motion derived from this equation takes on the form of the Mathieu equation, which is a linear second-order ordinary differential equation:

$$\frac{d^2u}{d\zeta^2} + (a_u - 2q_u\cos(2\zeta))u(\zeta) = 0 \tag{2}$$

with $\zeta = \frac{\Omega_{RF}t}{2}$ and $u = x, y$ is the displacement. The parameters a and q are called the stability or trapping parameters given by:

$$a = \frac{4e\Phi_{dc}}{m\Omega_{RF}r_0^2} \tag{3}$$

$$q = \frac{2e\Phi_{ac}}{m\Omega_{RF}r_0^2} \tag{4}$$

Note further that $a_x = -a_y$ and $q_x = -q_y$ due to Laplace's equation [13]. Of interest are regions of stability within this equation. Stability, in this case, means keeping an ion's trajectory within the trapping potential; instability would eject the ion.

From this statement, there are three simulations that are of interest:

1) Solving for Stable Solutions: It is of interest to determine the regions of stability given the parameter space of a and q. These stability charts are known as Ince-Strutt diagrams, and can be generated with numerical solvers or tables of Mathieu coefficients. With the region simulated, real values are provided to solve the Mathieu equation in the stable region. Analytical solutions exist, but for purposes of this course a numerical approach is used. Other solution methods are discussed.

2) Bounded and Unbounded Motion: To further prove stability, several parameter pairs can be solved and plotted to show the difference between bounded and unbounded particle motion within the trap. These are solved numerically.

3) Simulation of the Time-Average Electric Field: Once a stable solution is found, real-world values are applied to the aforementioned equations in order to simulate the electric field at the center of a quadrupole trap. This will prove the stability of a trapped charge. A discussion of different configurations is explored for the quadrupole trap as well.

III. Computational Methods and Results

This section covers each of the aforementioned problem spaces in order to advise and simulate the design of a linear quadrupole Paul trap. Figure 3 depicts the trap geometry targeted for this study. The x-axis defines the cross-sectional plane, with r as the radial distance from electrode to the ion. The z-axis is known as the trap-axis and contains the cylindrical electrodes where chains of multiple ions could be trapped together. Across each diagonal the RF source is shared, operating at Ω_{RF} frequency and Φ_{AC} amplitude. The opposite diagonal is phase offset by 180° and thus of equal and opposite voltage at any time t. A DC electric field is applied through the trap axis at Φ_{DC}.

Next, the simulation or algorithm is discussed, as well as parameters used to optimize the program. Finally, each section includes their individual results, as each part is advised by its predecessor.

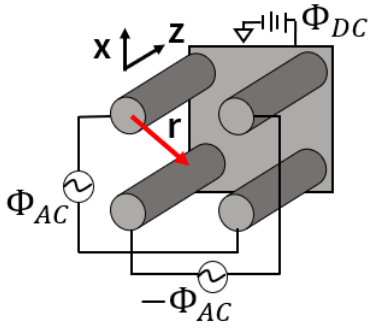

Fig. 3. Trap geometry for this work.

A. Stable Solutions to the Mathieu Equation

Stability for the Mathieu equation can be determined via a variety of methods. For this study, a numerical approach is used with Floquet theory [14]. Other techniques include perturbation and harmonic balancing but are outside the scope of this work. First, the Mathieu equation 2 can be arranged into a generalized Hill form:

$$\frac{d^2y}{dt^2} + f(t)y = 0 \tag{5}$$

$$f(t) = a - 2 * q\cos(t) \tag{6}$$

Let $y_1 = y$ and $y_2 = \frac{dy}{dt}$. Equation 5 can then be re-written as follows:

$$\frac{d}{dt}\begin{bmatrix} y_1 \\ y_2 \end{bmatrix} = \begin{bmatrix} 0 & 1 \\ -f(t) & 0 \end{bmatrix}\begin{bmatrix} y_1 \\ y_2 \end{bmatrix} \tag{7}$$

With this formulation, it is desired to create the fundamental solution matrix C given two sets of initial conditions out to an integration time T. If the fourth-order Runge-Kutta (RK4) method is used, and a solver can be thought of as having N steps to an arbitrarily long T integration time in order to generate some function f(t). T should be longer than one RF period, as it needs to capture artifacts that exponentially increase that may not exist at shorter integration times. The RK4 algorithm can be generalized to operate on some function $f''(t)$ as follows:

$$RK4\left(T, \begin{bmatrix} f(0) \\ f'(0) \end{bmatrix} = \begin{bmatrix} f_0 \\ f_0' \end{bmatrix}\right) = \begin{bmatrix} f(t) \\ f'(t) \end{bmatrix} \tag{8}$$

In equation 8, f_0 and f_0' represent the initial conditions for the function to be solved, $f''(t)$, out to some integration time T with adequate steps N. Let y_{11}, y_{12}, y_{21}, and y_{22} be constructed such that

$$RK4\left(T, \begin{bmatrix} y_{11}(0) \\ y_{12}(0) \end{bmatrix} = \begin{bmatrix} 1 \\ 0 \end{bmatrix}\right) = \begin{bmatrix} y_{11}(t) \\ y_{12}(t) \end{bmatrix} \tag{9}$$

$$RK4\left(T, \begin{bmatrix} y_{21}(0) \\ y_{22}(0) \end{bmatrix} = \begin{bmatrix} 0 \\ 1 \end{bmatrix}\right) = \begin{bmatrix} y_{21}(t) \\ y_{22}(t) \end{bmatrix} \tag{10}$$

Now the fundamental solution matrix C can be found by evaluating $y_{11}(t)$, $y_{12}(t)$, $y_{21}(t)$, and $y_{22}(t)$ at time T:

$$C = \begin{bmatrix} y_{11}(T) & y_{21}(T) \\ y_{12}(T) & y_{22}(T) \end{bmatrix} \tag{11}$$

From Floquet theory and as noted in [14], stability stems from the eigenvalues of C. The solutions for the eigenvalues can be found as

$$\lambda_{1,2} = \frac{tr(C) \pm \sqrt{trC^2 - 4}}{2} \tag{12}$$

From equation 12, consider the case where $|trC| > 2$. The roots are then real, but the product must be unity. That means that if one root is less than unity, the other must be greater than unity which indicates that there is exponential growth in time. With this now known, different parameters a and q can be substituted into equation 5 and solved to determine stability.

1) Simulation Setup: An adequately large integration time T is chosen to establish exponential growth. A time step dt is needed to generate the numerical solution out to time T as well. For a and q a range is given as well as number of points for the grid N to construct an NxN matrix of a, q pairs. These ranges are looped over to generate every possible a, q pair with some step a, q_{min} to a, q_{max} with step size $\frac{a,q_{max}-a,q_{min}}{N}$. Each pair is solved following equations 9 and 10, and then a solutions matrix of the last elements is created. The trace of the solutions matrix is found and compared with an integration error parameter, noted as err. Figure 4 shows a flowchart that depicts the process used to generate the results in this work. Table I contains the variable values used for the results.

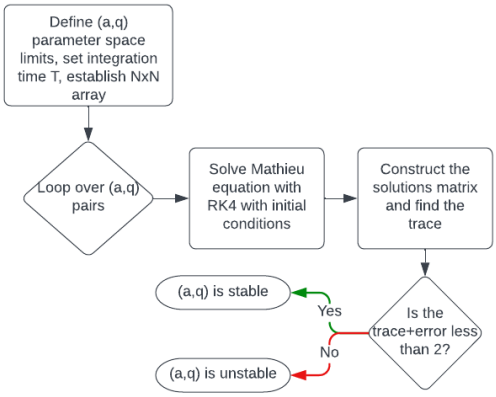

Fig. 4. Simulation flowchart for construction of the Ince-Strutt or stability diagram.

TABLE I
DEFINED VARIABLES FOR INCE-STRUTT SIMULATION.

Variable Name	Data Value
a, q_{min}	0
a, q_{max}	5
N	100
T	100 s
dt	.01 s
err	20

2) Results & Analysis: Figure 5 shows the resulting Ince-Strutt diagram. The simulation shows at least three distinct regions, called tongues, of stable parameter space. The boundaries between stable and unstable parameters mathematically

align to pairs where $|trC| = 2$ from equation 12. Unfortunately, due to constraints in the computing power available at the time of simulation, only a 100x100 sample grid was viable, and a, q pairs from 0 to 5 were used to show a few tongues of stable solutions. With more points, the curvature boundaries of these regions would extend to zero. Further, the numerical solutions found using Floquet theory can take more processing time than other methods, such as the perturbation method and harmonic balancing [14]. Analytical solutions also exist for the Mathieu equation [15] [16].

Comparing this to Figure 6, it is clear that with a higher resolution, the stability region boundaries would extend to $q = 0$.

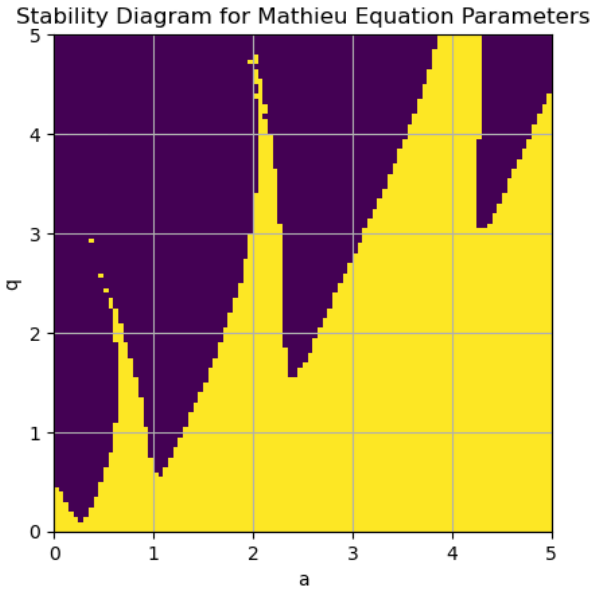

Fig. 5. Ince-Strutt diagram for a, q pairs from 0 to 5 with $err = 20$. The yellow regions indicate stable parameter pairs, while the purple indicates unstable pairs.

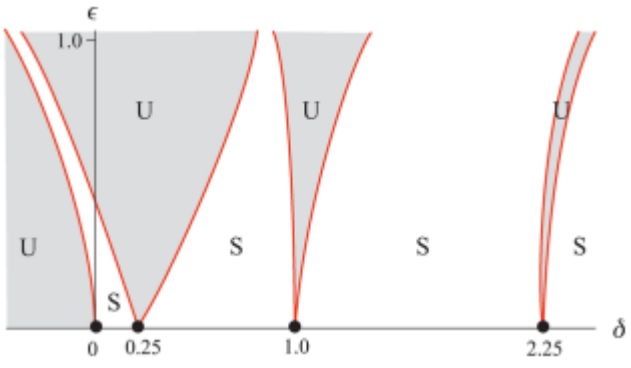

Fig. 6. Ince-Strutt diagram for ϵ, δ pairs from $\delta = 0$ to 2.25. Image source: [14].

B. Particle Motion within Solution Parameter Space

For this section, two parameters are chosen from the stability diagram in Figure 5. The goal is to show a case of bounded and unbounded motion, respectively.

1) Simulation Setup: For two pairs of a, q, the RK4 method is used to find the position and velocity of the particle. The parameters chosen should be from the stable and unstable regions in Figure 5. Table II shows the variable values used for this simulation. Bounded motion, in this sense, means that as t approaches infinity, the motion of the trapped particle remains periodic. Unstable parameters should eventually lead to exponential increase in particle motion. In reality, the motion becomes unsustainable within the potential and thus ejects the particle from the trap.

TABLE II
DEFINED VARIABLES FOR BOUNDED AND UNBOUNDED MOTION SIMULATION.

Variable Name	Data Value
$(a, q)_{bounded}$	$(2, 2)$
$(a, q)_{unbounded}$	$(3, 5)$
N	10000
T	20 s
dt	2 ms

2) Results & Analysis: With (a, q)=$(2, 2)$, the motion of the particle should stay bounded as t increases, as shown in Figure 5 and proved with Figure 7. Similarly, for (a, q)=$(3, 5)$, the particle motion should exponentially increase as t increases. A dramatic case in shown in Figure 8. It is interesting to note that this is an example of an undamped Mathieu equation. As an example, let's modify equation 2 to create the damped Mathieu equation [17]:

$$\frac{d^2u}{d\zeta^2} + b_u\frac{du}{d\zeta} + (a_u - 2q_u\cos(2\zeta))u(\zeta) = 0 \qquad (13)$$

This new term, $b_u\frac{du}{d\zeta}$, represents a dissipation factor over time, and thus the motion would decay as time t increases. Mechanically, this could be friction, or any other dissipative factor. Ince-Strutt diagrams become much more complicated, with numerical solutions at long integration times used to solve for stability parameters. However, for the case of an RF Paul trap, no major dissipative forces play a role, save for stray electric fields present near the trapped ion. Thus, the undamped Mathieu equation provides a better model for motion within the trap.

C. Electro-Static Fields for Trap Geometry

Allowing (a, q)=$(2, 2)$, real values can now be plugged in to find the voltages necessary to obtain the geometry shown in Figure 3. Further, Ω_{RF} is chosen to be 1MHz, a common trap frequency. Note further that equations 3 and 4 can be rearranged as follows:

$$\frac{qm\omega^2}{2e} = \frac{\Phi_{AC}}{r_0^2} \qquad (14)$$

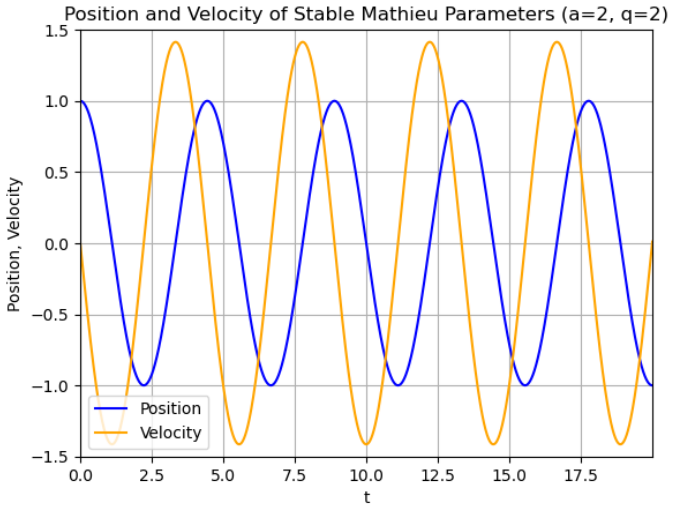

Fig. 7. Bounded motion for (a, q)=$(2, 2)$. The units for position and velocity can be considered arbitrary, as they can be scaled to match the parameters of a chosen trap geometry from equations 3 and 4.

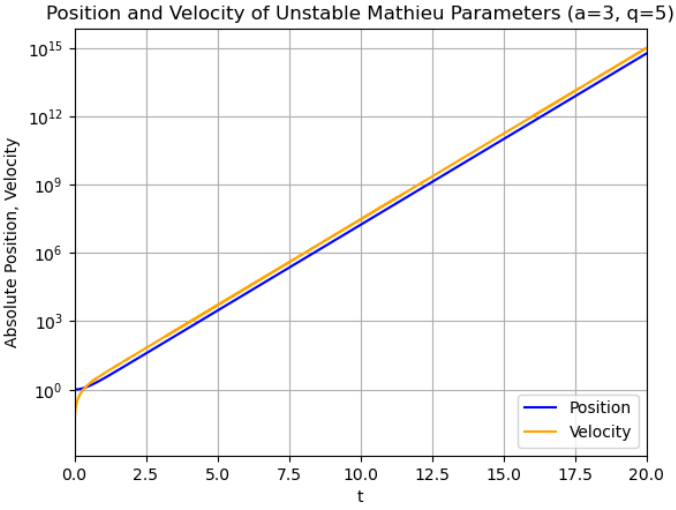

Fig. 8. Unbounded motion for (a, q)=$(3, 5)$. Note the exponential increase in position compared with the same time period for Figure 7.

$$\frac{am\omega^2}{4e} = \frac{\Phi_{DC}}{r_0^2} \tag{15}$$

Thus, Φ_{DC} must be a factor of 2 less than Φ_{AC} if $a = q$. Selecting $\Phi_{AC} = 100V$ then leads to $\Phi_{DC} = 50V$, which are easily realizeable with laboratory equipment. These calculated trap values are tabulated in Table III.

As shown in class, the electric potential can be found given Gauss's Law:

$$\nabla\phi = \frac{\partial^2\phi}{\partial x^2} + \frac{\partial^2\phi}{\partial y^2} + \frac{\partial^2\phi}{\partial z^2} = 0 \tag{16}$$

This time-independent problem can be solved as boundary value problem for a charge density at the given timestep.

TABLE III
CALCULATED PARAMETERS FOR ELECTRO-STATICS SIMULATION.

Variable Name	Data Value
$(a, q)_{bounded}$	$(2, 2)$
Ω_{RF}	1 MHz
Φ_{AC}	100 V
Φ_{DC}	50 V
m_{Ca+}	$6.64 * 10^{-19}$ kg
e	$1.6 * 10^{-19}$ c

1) Simulation Setup: For the first time step, the cylindrical rods are given a charge density based on the voltage amplitude, Φ_{AC}. Next, Jacobi's method is used to solve for the 2D partial differential equation 16. Table IV shows the simulation variables used for this section. At the very end of the simulation, Φ_{DC} is added to every point, representing the compensation electrode that occurs across the entire trap. The cylindrical rod radius was chosen to be relatively small to emulate a manufacturable cylinder used in experiments. This radius is on the order of $10\mu m$.

TABLE IV
DEFINED VARIABLES FOR ELECTRO-STATICS SIMULATION.

Variable Name	Data Value
$(a, q)_{bounded}$	$(2, 2)$
d	$(3, 5)$
N	100
T	.16 us
dt	1.6 ns
$target$	$1*10^{-6}$
ϵ_0	$8.85*10^{-10}$

2) Results: Figure 9 shows the simulation created for the electro-static potentials. It is clear that the center of the trap experiences a net zero electric potential. Elsewhere, the compensation DC field persists, which should help confine the electrode. Other equipotential areas persist outward from the center of the trap, which is less desired. Discussion on how to improve this can be found in Section IV.

IV. FUTURE WORK & LIMITATIONS

Many of the incurred problems came from running simulations with lengthy runtimes for higher resolution. Figure 5 took over an hour to process as each point involved solving two initial value problems using the RK4 method. With access to the cluster, this could easily be made to run on parallel cores with as many nodes as possible for incredible speedup in operation. Then, with a higher resolution grid, the curves of the stability plot would be more evident, as well as a larger plot including higher values of a, q could be explored. Further future work on the Ince-Strutt diagram could easily include a comparison of the Floquet theory approach accuracy to the harmonic balancing or perturbation approaches used in other works. The curves that serve as the boundaries between stable and unstable solutions also have deterministic equations, so each could be compared quite easily. However, time would

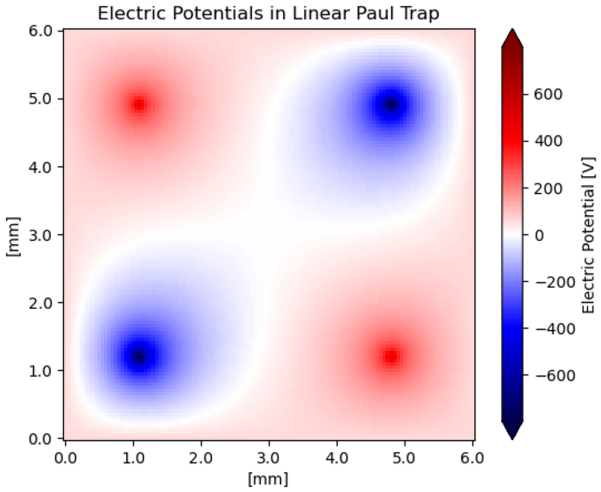

Fig. 9. Electric potential at time step 0 in the simulation.

not allow the exploration of these methods within the scope of an individual project.

A large error was needed for the Floquet theory approach. This could have been necessary due to the use of a short integration time in the initial conditions or due to the use of the Floquet theory in general compared to perturbation. With more computing power, a longer integration time could be used.

Trap geometry plays an important role in the parameters for a Paul trap. It can be clearly seen in Figure 9 that there are relaxed electric potentials in a cross formation between each electrode extending outwards from the ion position. These can be escape points without strong enough DC confinement. This can be alleviated with hyperbolic electrodes which "squeezes" these equipotential areas and thus improves confinement of the particle. Different trap geometries could definitely be explored in future work, with emphasis on determining the effect of hyperbolic electrodes on the confining potential.

While cylindrical electrodes are simple in implemenetation, many ion trapping groups use planar electrodes. Mesh analysis is used to create a similar electric potential well to Figure 9. Solving methods for many planar traps has been extensively explored as they are easy to microfabricate and show promising configurations for a trapped ion based quantum computer.

V. Conclusion

Three simulations were performed in order to advise the design of a linear RF Paul trap.

The first simulation created an Ince-Strutt diagram to determine stable parameters of a and q that would eventually decide trap voltages, frequencies, and radial distances for the ion. The RK4 method was used to solve two initial value problems for the second-order linear differential Mathieu equation, which describes the particle motion within the trap. This involved the use of Floquet theory to easily determine unbounded behavior without the need for long integration times. The results were successful, with a characteristic Mathieu stability diagram being created.

With the stability diagram as a guide, two (a, q) parameter pairs were chosen to demonstrate both bounded and unbounded particle motion. This involved using the RK4 method to solve each equation for a relatively small integration time in order to prove stability. The results were succesful, with a clear exponential increase in particle motion for the unbounded case.

Finally, a quadrupole trap was simulated based on the stability parameters from each step. Using a trap frequency of 1MHz, trap variables such as AC and DC voltage were found based on the Ca^+ mass and charge ratio. These voltages were realizeable numbers that could be achieved in a laboratory. The electro-static voltages were simulated based on Poisson's equations, the found voltages, and the radial distance of the ion from the cylindrical electrodes. This was done via the Jacobi method. The results were a clear equipotential well in the center of the trap, which proves that the chosen trap parameters worked for the stable solutions derived in previous steps.

References

[1] D. Rodríguez, "Mats and laspec: High-precision experiments using ion traps and lasers at fair," *The European Physical Journal Special Topics*, vol. 183, pp. 1–123, May 2010.

[2] C. J. Ballance, T. P. Harty, N. M. Linke, M. A. Sepiol, and D. M. Lucas, "High-fidelity quantum logic gates using trapped-ion hyperfine qubits," *Phys. Rev. Lett.*, vol. 117, p. 060504, Aug 2016.

[3] M. H. Holzscheiter, "A brief history in time of ion traps and their achievements in science," *Physica Scripta*, vol. 1995, p. 69, Jan 1995.

[4] Z. D. Romaszko, "Engineering of microfabricated ion traps and integration of advanced on-chip features," *Nature Reviews Physics*, vol. 2, pp. 285–299, Jun 2020.

[5] J. P. Home, "Chapter 4 - quantum science and metrology with mixed-species ion chains," in *Advances in Atomic, Molecular, and Optical Physics* (E. Arimondo, P. R. Berman, and C. C. Lin, eds.), vol. 62 of *Advances In Atomic, Molecular, and Optical Physics*, pp. 231–277, Academic Press, 2013.

[6] J. Labaziewicz, Y. Ge, P. Antohi, D. Leibrandt, K. R. Brown, and I. L. Chuang, "Suppression of heating rates in cryogenic surface-electrode ion traps," *Phys. Rev. Lett.*, vol. 100, p. 013001, Jan 2008.

[7] M. C. Revelle, "Phoenix and peregrine ion traps," *arXiv preprint arXiv:2009.02398*, 2020.

[8] T. G. Ballance, J. F. Goodwin, B. Nichol, L. J. Stephenson, C. J. Ballance, and D. M. Lucas, "A short response time atomic source for trapped ion experiments," *Review of Scientific Instruments*, vol. 89, no. 5, p. 053102, 2018.

[9] M. Vogel, "Particle confinement in penning traps," *Springer Series on Atomic, Optical, and Plasma Physics*, vol. 100, 2018.

[10] K. G. Libbrecht and E. D. Black, "Improved microparticle electrodynamic ion traps for physics teaching," *American Journal of Physics*, vol. 86, no. 7, pp. 539–558, 2018.

[11] D.-I. ho, S. Hong, M. Lee, and T. Kim, "A review of silicon microfabricated ion traps for quantum information processing," *Micro and Nano Systems Letters*, vol. 3, pp. 1–12, 2015.

[12] A. Drakoudis, M. Söllner, and G. Werth, "Instabilities of ion motion in a linear paul trap," *International Journal of Mass Spectrometry*, vol. 252, no. 1, pp. 61–68, 2006.

[13] R. E. March, R. J. Hughes, and J. F. Todd, *Quadrupole storage mass spectrometry*. John Wiley & Sons, 1989.

[14] I. Kovacic, R. Rand, and S. M. Sah, "Mathieu's equation and its generalizations: Overview of stability charts and their features (review article)," *Applied Mechanics Reviews*, vol. 70, p. 020802, 03 2018.

[15] E. I. Butikov, "Analytical expressions for stability regions in the Ince–Strutt diagram of Mathieu equation," *American Journal of Physics*, vol. 86, pp. 257–267, 04 2018.

[16] D. J. Daniel, "Exact solutions of Mathieu's equation," *Progress of Theoretical and Experimental Physics*, vol. 2020, 04 2020. 043A01.
[17] J. H. Taylor and K. S. Narendra, "Stability regions for the damped mathieu equation," *SIAM Journal on Applied Mathematics*, vol. 17, no. 2, pp. 343–352, 1969.